Nat Hazards (2016) 82:1279–1300
DOI 10.1007/s11069-016-2243-y

ORIGINAL PAPER

Rainfall-runoff modelling using a spatially distributed electrical circuit analogue

Khodayar Abdollahi[1] · Pablo Guzmán[1,2,3] · Marijke Huysmans[1] · Okke Batelaan[4]

Received: 21 September 2015 / Accepted: 10 February 2016 / Published online: 22 February 2016

Abstract The assessment and prevention of floods require appropriate forecasting and knowledge of the related hydrological processes. Due to the similar form of the governing equations, flood hydrograph shows a clear analytical and mathematical analogy with electrical circuits. In this paper, a spatially distributed hydrological model is developed which is analogue to a network of electrical resistance–capacitance with five circuits for describing the hydrological processes leading to floods. The spatially distributed hydrological model simulates rainfall, potential evapotranspiration, canopy interception, surface storage and soil storage. The parameters for analogical modelling were derived from translation of the physical catchment characteristics. A two-parameter Weibull equation aggregates the response functions of each pixel and calculates the hydrograph of the catchment. We applied the model to the 'Open-Book' or 'tilted V-catchment' theoretical benchmark problem, as well as to four hourly flood events and simulation of daily discharges. For the last two cases, data were used from the mountainous catchment of upper Tarqui in the Andes of Ecuador. Comparison of single versus multiple circuit designs for the benchmark problem indicates that the multiple circuit analogy provides a result similar to other hydrological models. The results further illustrate the usefulness of the methodology for flood modelling and how it can simplify the simulation for ungauged basins of temporal and spatial variations of influencing hydrological processes.

Keywords Flash flood · Electrical circuit analogy · Weibull distribution · Distributed modelling

✉ Khodayar Abdollahi
kabdolla2010@gmail.com

[1] Department of Hydrology and Hydraulic Engineering, Vrije Universiteit Brussel, Brussels, Belgium

[2] Programa de Manejo de Agua y Suelo, PROMAS, Universidad de Cuenca, Cuenca, Ecuador

[3] Department of Earth and Environmental Sciences, KU Leuven, Celestijnenlaan 200e, Bus 2410, 3001 Heverlee, Belgium

[4] School of the Environment, Flinders University, GPO Box 2100, Adelaide, SA 5001, Australia

1 Introduction

Large areas around the world are prone to floods due to various factors such as high percentage of impervious surface, receiving intensive rainfall and having steep slopes (Berz et al. 2001; Barredo 2007; Hapuarachchi et al. 2011). This type of hazards often occurs within a short time interval under conditions of a combination of heavy rainfall or rapid snowmelt and high soil water content. Flash floods may also happen as a result of human-related activities such as dam failures. Global assessment of the loss of human life has shown that flash floods cause the highest rate of mortality per event (Jonkman 2005). Due to the importance of threats of floods for communities, the hydrological aspects of flood forecasting have been intensively studied in the past decades based on the advances in the underlying laws of hydrological systems (HS). Sherman (1932) developed the unit hydrograph concept to estimate the hydrological response to rainfall. Horton (1933) introduced the infiltration theory for modelling rainfall excess. After their work, new advances in computational methods and observation capabilities kept flash floods and flood modelling on the research agenda (Costa 1987; Jarrett 1987; Brath and Rosso 1993; Yates et al. 2001; Ferraris et al. 2002; Foody et al. 2004; Gaume et al. 2004; Anquetin et al. 2005; Mariani et al. 2005; Amengual et al. 2007; Reed et al. 2007; Norbiato et al. 2007; Borga et al. 2007; Blöschl et al. 2008; Ruiz-Villanueva et al. 2010).

It is difficult to find a clear difference between an ordinary flood and a flash flood (Georgakakos 1986), but flash floods exhibit particular behaviour. According to Anquetin et al. (2010), flood dynamics are characterized by two phases: the first mainly controlled by rainfall variability and the second, controlled by soil properties. Hence, rain and terrain are among the most influential factors in causing extreme floods. As an example, Marchi et al. (2010) stressed the importance of accounting soil water storage and its impact on runoff coefficients.

Attempts have been made to schematize HS behaviour by analogy with electrical systems (ES) (Chow 1964). Analogy serves as a logical base for having a better insight into the internal processes of two corresponding systems. The similarities between ES and HS lead to a direct correspondence between flood flows and the elements of the electrical circuit (Shen 1965). As the differential equations describing HS and ES have a similar form, similar responses can be expected. The volumetric discharge in HS shows a similar behaviour to the current in ES (Cannon 1967). There is also an analogy between voltage and the head of water (hydraulic potential).

These similarities reflect why different studies have been focused on the analogy between mathematical descriptions of different dynamic systems, e.g. electro-magnetic, electro-mechanic and electro-hydraulic (Kundzewicz 1987). Stark and Stark (2001) used a network of nonlinear resistors and capacitors to describe a spatial channelization model for soil erosion assessment. Collier (1998)introduced a lumped river electrical water analogue research and development (REWARD) model based upon an interpretation of inductance–capacitance–resistance circuits in terms of catchment parameters and physical processes. The advantage of choosing physically meaningful parameters for modelling is that calibration requirements of models can be reduced accordingly (Garrote and Bras 1995). A number of studies have performed laboratory analogue experiments for rainfall-runoff modelling. Laboratory simulations by Nourani et al. (2007) employed the Liquid Analogy Model (LAM) based on the continuity equation for flow and Darcy's law. LAM was proposed as an educational instrument, but it was tested for a real storm event as well (Nourani and Monadjemi 2006; Nourani et al. 2007). Recently, LAM has been applied for

distributed modelling of seepage phenomena under dams and embankments (Nourani et al. 2014a, b).

Figure 1 demonstrates how water balance components are represented as electrical resistance–capacitance (RC) circuits. Every component can be decomposed into a number of *equivalent electrical* resistance–capacitance *circuits*, representing hydrological processes. In this approach, each pixel of a gridded map is represented by an electrical circuit with five RC circuits.

The capacitor stores electrical charge and thus stores energy like water is stored in a reservoir. The maximum capacitance of a capacitor is the amount of charge (q) stored at a known voltage across two sides and measured as a farad (F), which equals to the charge in coulombs that it takes the potential across the capacitor to change 1 V (Eq. 3 in Table 1). Mathematically, the relation between stored electrical energy and voltage is given by Eq. 4 in Table 1. The sum of the voltage of the capacitor (V_C) and resistor (V_R) is the battery voltage (V_B):

$$V_B = V_R + V_C \tag{6}$$

This can be expressed in terms of the charge

$$V_B = \frac{dq}{dt}R + \frac{q}{C} \tag{7}$$

when $t = 0$ and $V_B = 0$ the charge $q(t)$ at time t will be

$$q(t) = q_{max}\left(1 - e^{\frac{t}{RC}}\right) \tag{8}$$

where q_{max} is the maximum charge on the capacitor. RC is the circuit's time constant (RC no. 5 Figure 1a) (min). As demonstrated in Fig. 2, this equation is analogous to the equation describing a single linear reservoir (Pedersen et al. 1980):

$$R_D = Pe\left(1 - e^{-\frac{t}{tl}}\right) \tag{9}$$

where R_D is runoff depth (mm), Pe is excess rainfall (mm) at time t(min), tl(min) is the storage lag time of the catchment, and hence, it is equivalent to RC in Eq. 8. If Q^* is the discharge when rainfall excess stops (m^3/s), the equation for the falling limb will be:

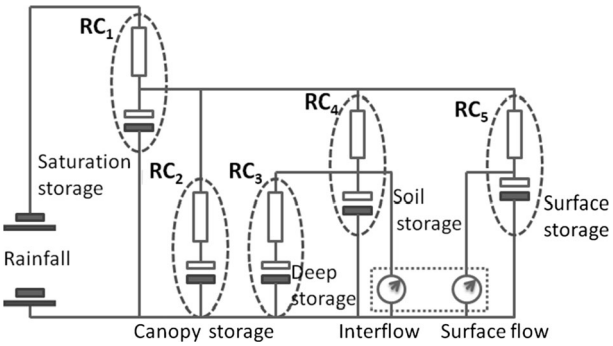

Fig. 1 Electrical circuit concept of a pixel. RC_x is a resistor–capacitor

Table 1 Physical relationship for RC circuit quantities

Quantity	Equation No.	Equation	Remarks
Current (I)	Equation 1	$I = \frac{q}{60 \times t}$	I in (Amp), q charge in (C), t time in (min)
Voltage (V)	Equation 2	$V = \frac{I}{R}$	V in (V), R resistance in (Ω)
Capacitance (C)	Equation 3	$C = \frac{q}{V}$	C in (F)
Energy (E)	Equation 4	$E = C\frac{V^2}{2}$	E in (J)
Time constant (τ)	Equation 5	$\tau = RC/60$	τ in (min)

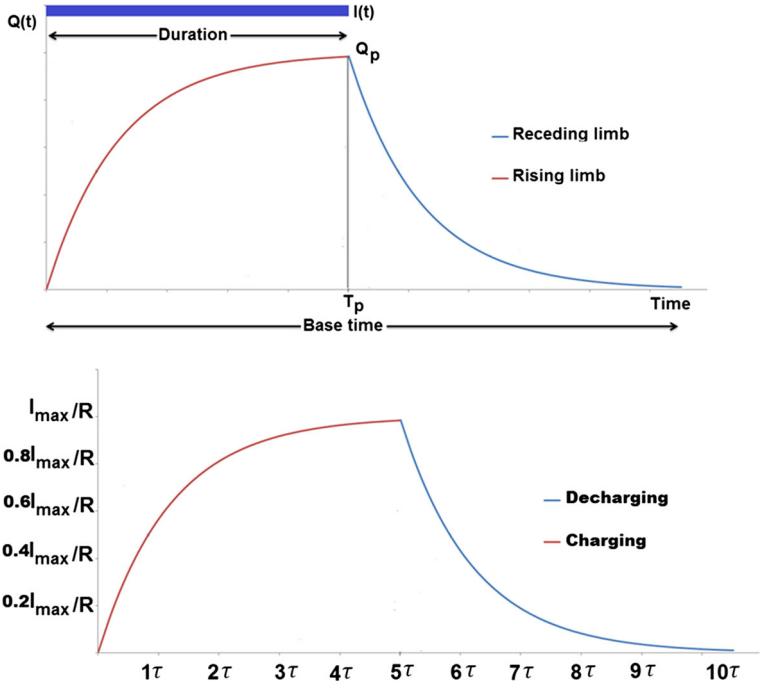

Fig. 2 Hydrograph due to a pulse of instantaneous input (*upper figure*). The behaviour is similar to the RC circuit's response to an electrical pulse (*lower picture*)

$$Q(t) = Q^* \mathrm{e}^{-\frac{t}{\eta}} \tag{10}$$

Our work aims at a methodological analogy with parameters that are meaningful in both HS/ES. We develop a spatially distributed form of the electrical analogy model as was suggested by Collier (1998). In areas with high spatial variability of hydrological parameters, lumped flood modelling is difficult (Laraque et al. 2007). In such cases, spatially distributed modelling can capture better the spatial variability of hydrological parameters that influence (flash) floods. The objective of this paper is to implement and test a novel approach for the HS/ES analogy as main element of a new spatially distributed open-source model 'Rain and Snow Accumulation Model' (RASAM).

2 Methods

2.1 Structure of the model

The model applies a grid approach to simulate the spatial distribution of interception, evapotranspiration, infiltration and surface runoff (Fig. 3). Input fluxes for each cell are assumed to generate an independent response function similar to its corresponding RC circuit (Fig. 1). Based on the HS-ES analogy, shape and scale parameters of Weibull are used to describe the exponential equations of hydrological processes (Table 2). The parameters are associated with rainfall and physical properties of the pixel, but shape parameter may also be influenced by the length of the flow path. To obtain the overall response, the response functions for all contributed time areas (isochronal map) are combined. It is possible to simplify Fig. 1 into a single RC. To find out whether selecting multi-circuit versus single structure improves the simulations or not, we applied both versions on a simplified topography. The single RC considers the pixel area as an RC circuit, while the second structure with multi-circuit (as part of RASAM) subdivides the system into five hydrological components (Fig. 1a). In RASAM, the water balance at the pixel scale is formulated as:

$$\frac{\Delta S}{P} = 1 - \frac{1}{P}(f_1(\mathrm{RC}_1) + f_2(\mathrm{RC}_2) + f_3(\mathrm{RC}_3) + f_4(\mathrm{RC}_4) + f_5(\mathrm{RC}_5)) \tag{11}$$

where ΔS is change in soil moisture (mm), P is precipitation (mm), the other terms are a function of the corresponding circuits (f_1–f_5) for evapotranspiration (RC_1), interception (RC_2), groundwater (RC_3), infiltration (RC_4) and surface runoff (RC_5) (Fig. 1a).

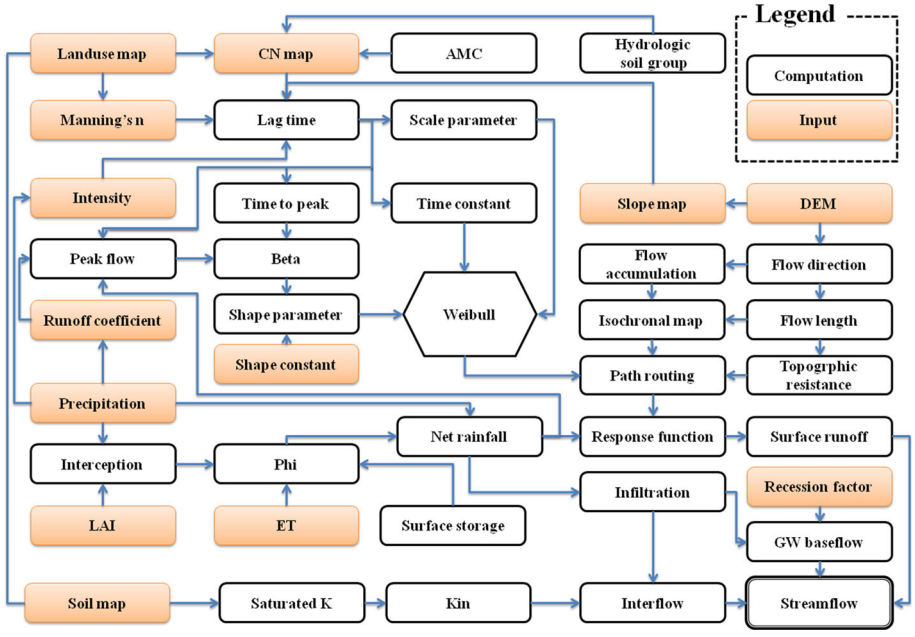

Fig. 3 Flow chart of the model structure (*coloured boxes* indicate inputs and the *box* with the *double border* represents the model output)

Table 2 Exponential form of water balance components in hydrological systems

Component	Equation No.	Exponential equation	Remarks
Interception (Intc)	Equation 15	$\text{Intc} = \frac{1}{24} C_P \text{SI}_{\max} \left(1 - e^{\frac{-24 k_C P_e}{\text{SI}_{\max}}}\right)$	Aston (1979)
Surface runoff (SR)	Equation 16	$\text{SR} = P(t)\left(1 - e^{-\frac{t}{tl}}\right)$	Pedersen et al. (1980)
Infiltration (F_c)	Equation 17	$F_c = f_C t + \frac{(f_0 - f_C)}{k}\left(1 - e^{\frac{-k_S t}{60}}\right)$	Horton (1933)
Actual ET (AET)	Equation 18	$\text{AET} = \text{ET}\left(1 - e^{-\frac{P_e}{\text{ET}}}\right)$	Schreiber (1904) Oudin et al. (2010)
Interflow (IF)	Equation 19	$\text{IF} = F_c\left(1 - e^{-K_{in}\frac{t}{tl}}\right)$	Based on surface runoff Eq. 16

Equation 15: C_P is the canopy cover fraction per pixel, $\text{SI}_{\max}$ is the maximum canopy storage capacity (mm/day), k_C is a parameter that determines the fraction of rainfall which falls on the canopy, P_e is the precipitation (mm/h); Eq. 16: $P(t)$ is excess precipitation (mm/h), t is time (min), tl is lag time of the cell (min); Eq. 17: f_C is final infiltration rate (mm/h), f_0 is initial infiltration (mm/h), t is time from beginning of storm (min), k_S is decay coefficient (1/min); Eq. 18: ET is potential evapotranspiration (mm/day); Eq. 19: K_{in} is dimensionless drainage characteristic, t and tl as in Eq. 16

And

$$\begin{cases} P = F_c + \text{AET} + \text{SR} + \text{Intc} \\ \Delta S = F_c - \text{IF} - (\text{BF} + \text{GWR}) \end{cases} \tag{12}$$

where F_c denotes effective infiltration (mm), SR is surface runoff (mm), Intc is interception (mm) and AET is actual evapotranspiration (mm),IF is interflow (mm), GWR and BF are groundwater inflow (mm) and outflow (baseflow) (mm), respectively.

2.1.1 Interception

The interception [Intc (mm)] component is expressed (Eq. 15 in Table 2) by Aston's model (1979) which uses a dimensionless leaf area index (LAI), and it also takes the exponential relation with storage into account. k_C in Eq. 15 is a parameter that determines the fraction of rainfall which falls on the canopy, it has a linear relationship with the leaf area index (De Jong and Jetten 2007):

$$k_C = 0.065 \text{ LAI} \tag{13}$$

The maximum canopy storage capacity ($\text{SI}_{\max}$) (Eq. 15 in Table 2) is estimated from LAI (Von Hoyningen-Huene 1981; de Jong and Jetten 2007):

$$\text{SI}_{\max} = 0.935 + (0.498 * \text{LAI}) - \left(0.00575 * \text{LAI}^2\right) \tag{14}$$

2.1.2 Evaporation

RASAM considers pan evaporation as Potential evapotranspiration (ET). In case of water limitation, ET can be simulated using a simplified version of the Penman–Monteith formula based on a combination of an energy balance with a mass transfer method (Valiantzas 2006). Depending on the ratio between precipitation (P) and evaporation, ET is actualized as AET using equation Eq. 18.

2.1.3 Infiltration

Infiltration (Eq. 17 in Table 2) is calculated by a combined Horton-SCS scheme (Gabellani et al. 2008). Infiltration rate at the beginning of rainfall is high, but it decreases over time exponentially (Horton 1933). The potential maximum soil retention (S_p (mm)) represents infiltration occurring after runoff. The model uses an empirical potential maximum storage formulation (SCS 1985):

$$S_p = \frac{25400}{CN} - 254 \tag{20}$$

where CN is the NRCS (US Department of Agriculture, Natural Resources Conservation Service, formerly known as the Soil Conservation Service) curve number.

2.1.4 Surface runoff component

Surface runoff is formulated (Eq. 16 in Table 2) based on Pedersen et al. (1980) and is calculated under the condition that if the net rainfall rate exceeds the infiltration rate, runoff will be initiated. For simplification, the total losses (in view of surface runoff processes) can be summed up in a new parameter φ (mm/h).

$$\varphi = F_c + \text{Intc} + \text{AET} \tag{21}$$

This threshold acts as a switch for rainfall events that result in runoff. F_c is effective infiltration (mm/h), Intc and AET are, respectively, hourly interception rate (mm/h) and actual evapotranspiration (mm/h). The starting time of excess rainfall is controlled by φ. The lag time for each pixel is the difference between the centre of mass of rainfall excess and direct runoff. Melesse et al. (2007) showed that the travel time through a pixel (tl_c) in minutes is given as:

$$tl_c = 7\left(\frac{n \times L}{I_{in}^{\frac{2}{3}} S_l^{\frac{1}{2}}}\right)^{\frac{3}{5}} = \frac{7 \times n^{0.6} L^{0.6}}{I_{in}^{0.4} S_l^{0.3}} \tag{22}$$

$$I_{in} = (i - \varphi) \tag{23}$$

n is Manning's roughness coefficient,L length of flow path (m), S_l average overland flow path slope (m/m), I_{in} Hortonian direct rainfall (mm/h), i rainfall intensity (mm/h) and φ expressed in the same unit as intensity $i > \varphi$. The required time until the whole catchment contributes to runoff is the time of concentration which is assumed here to be equal to the time to peak flow. For a uniform intensity of I_{in}(mm/h) as rainfall excess, the peak flow [q_p (m^3/s)] is calculated as (adopted from Pedersen et al. 1980):

$$q_p = 2.78 \times 10^{-7} \times C_R A_c I_{in} \left[1 - \exp\left(-\frac{t_r}{t_l}\right)\right] \tag{24}$$

where C_R is runoff coefficient, A_c is the contributing area to runoff generation (m^2), t_r is duration of storm (min) and t_l is lag time of the cell (min), respectively.

2.1.5 *Interflow*

RASAM conceptualizes the soil profile in three layers. The first layer is a surface layer of 5 cm thickness, all infiltration processes occur in this layer. The second layer with 25 cm thickness is the layer in which interflow is conceptualized. The main reason for this simplification is related to the fact that most of the daily soil water dynamics occurs in the first 25–30 cm of the soil profile (Rawlins et al. 2013). The deepest layer is the groundwater zone. The behaviour of the lateral movement of water in the second layer is considered as irrigated surface water that returns again to surface runoff with lower velocity. To model interflow, a dimensionless drainage characteristic (k_{in}) (Sheikh et al. 2009) was defined based on saturated hydraulic conductivity [K_{sat} (mm/day)]:

$$k_{\text{in}} = 0.0866\, e^{0.8063 \log_{10} K_{\text{sat}}} \quad 0 < k_{\text{in}} < 1 \tag{25}$$

The coefficient is used as a proportional factor for the lag time in the formulation of interflow (Eq. 19 in Table 2).

2.1.6 *Response functions*

The Weibull equation (Weibull 1951) was used to sum charging and discharging phases of the RC circuits over time. This equation is selected because of its closeness to the distribution of electrical RC response (Agarwal et al. 2003; Liu et al. 2002), and because the density function of the Weibull distribution can be directly translated into the response of the pixels. Table 3 shows a summary of the most important properties of the Weibull distribution. The Weibull distribution has a flexible density function with two parameters (in addition to time). The scale parameter ($\hat{a}$) determines shrinking and widening of the shape of hydrograph by changing the range of the distribution. The Weibull shape parameter $\hat{b}$ is responsible for the shape of the response function as illustrated by Fig. 4. The Weibull distribution has been widely used in hydrology (Bhunya et al. 2007; Pramanik

Table 3 Summary of some properties of the Weibull distribution

Property	Equation No.	Formula	Remarks
PDF (−)	Equation 29	$F = 1 - \exp\left(-\left(\frac{t}{\hat{a}}\right)^{\hat{b}}\right)$	Liu et al. (2002)
Impulse response (1/min)	Equation 30	$h = \left(\frac{\hat{b}}{\hat{a}}\right)\left(\frac{t}{\hat{a}}\right)^{\hat{b}-1}$	$\frac{\text{Density function}}{\text{Storage function}}$
Storage function (m^3)	Equation 31	$S = \exp - \left(\frac{t}{\hat{a}}\right)^{\hat{b}}$	$\frac{\text{Density function}}{\text{Impulse response}}$
Density function (m^3/s)	Equation 32	$q(t) = \frac{V_f}{60}\left(\frac{\hat{b}}{\hat{a}}\right)\left(\frac{t}{\hat{a}}\right)^{\hat{b}-1}\exp\left(-\left(\frac{t}{\hat{a}}\right)^{\hat{b}}\right)$	Rai et al. (2009)
Peak (m^3/s)	Equation 33	$q_p = \frac{V_f}{60}\left(\frac{\hat{b}}{\hat{a}}\right)\left(1-\frac{1}{\hat{b}}\right)^{1-\frac{1}{\hat{b}}}\exp\left(-\left(1-\frac{1}{\hat{b}}\right)\right)$	Pramanik et al. (2010)
Time to peak (min)	Equation 34	$t_p = \hat{a}\left(1-\frac{1}{\hat{b}}\right)^{\frac{1}{\hat{b}}}$	Pramanik et al. (2010)
First moment (min)	Equation 35	$\tau = \hat{a}\Gamma\left(1+\frac{1}{\hat{b}}\right)$	Liu et al. (2002)
Second moment (min)	Equation 36	$\sigma^2 = \hat{a}\left[\Gamma\left(1+\frac{2}{\hat{b}}\right) - \Gamma^2\left(1+\frac{1}{\hat{b}}\right)\right]$	Liu et al. (2002)

Parameters: t is time (min), a is a scale parameter (min), b is shape parameter (−), V_f is flow volume (m^3) and Γ is a gamma function

et al. 2010; Rai et al. 2009). Since the basis of this methodology was founded on the electro-hydraulic analogy, our current implementation differs from previous studies. It can be noticed that for an area of one square kilometre, the runoff coefficient equals to one, a time to peak of an hour and an intensity of rainfall of 5 mm per hour, the NRCS hydrograph corresponds to $\hat{a} = 78$ (min) and $\hat{b} = 2.4$ in formulation for Weibull distribution (Fig. 4(Right)).

Combining Eqs. 32 and 33 yields the dimensionless Weibull distribution as

$$\frac{q(t)}{q_p} = \left(\frac{t}{t_p}\right)^{\hat{b}-1} \exp\left[\left(1-\frac{1}{\hat{b}}\right)\left(1-\left(\frac{t}{t_p}\right)^{\hat{b}}\right)\right] \tag{26}$$

which does not require scale parameter. A non-dimensional parameter β is defined as the inverse product of q_p and t_p:

$$\hat{\beta} = t_p \times q_p = \left(\hat{b}-1\right)\exp\left[\left(\frac{1}{\hat{b}}-1\right)\right] \tag{27}$$

After taking the natural logarithm of both sides, one obtains:

$$\hat{b} = \frac{1}{\ln\left[\frac{\hat{\beta}}{\hat{b}-1}\right]+1} \tag{28}$$

The catchment scale analysis of Rai et al. (2009) on 13 different sized catchments having different climate and physiographic characteristics showed that the shape parameter $\hat{b}$ varies from 0.99 to 2.54.

Bhunya et al. (2007) suggested a trial-and-error procedure to estimate the shape parameter. Considering the computational time needed for spatial parameter estimation, a nonlinear regression (on pair shape parameters that produces an area under curve equal to one) has been adapted to estimate the shape parameter ($r^2 = 0.99$):

$$\hat{b} = \left(\hat{\alpha}\hat{\beta}+1\right)^2 \tag{37}$$

$\hat{\alpha}$ depends on the pixel size and average properties of catchment. This parameter is considered to be the same for all pixels. The actual value for gauged catchments can be

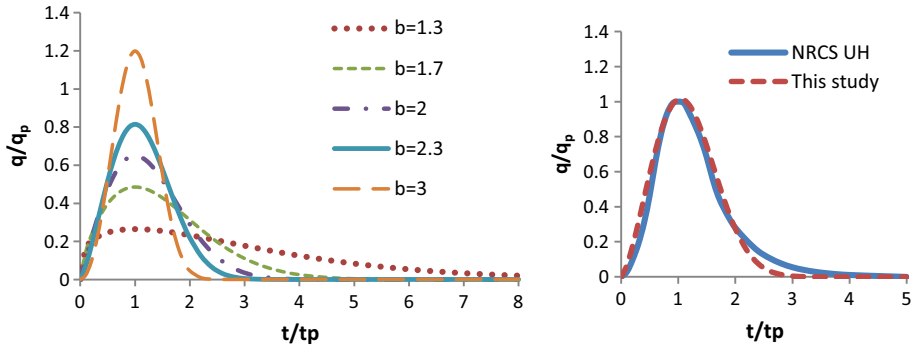

Fig. 4 *Left* Effect of the shape parameter $\hat{b}$ on the dimensionless hydrograph. *Right* Comparison of NRCS unit hydrograph (UH) (*full line*) with derived unit hydrograph using Weibull distribution (*dashed line*)

obtained through calibration. Substitution of b in time of peak gives the initial scale parameter (a):

$$\hat{\alpha} = \frac{t_{\mathrm{p}}}{\left(1 - \frac{1}{b}\right)^{\frac{1}{b}}} \tag{38}$$

2.1.7 Streamflow

Streamflow is calculated as the volumetric sum of baseflow and surface runoff. The effect of the flow path is applied by changing the parameter λ which synthetically accounts for the effects of flow path routing on the shape parameter. By using λ parameter, the initial shape parameter b_1 is transformed into a new modified shape parameter:

$$\hat{b}_2 = \lambda \hat{b}_1 \tag{39}$$

where b_2 is the modified shape parameter. To calculate the new parameter after this change, the mean (first moment) of the initial response and routed function must be equal.

$$\hat{a}_1 \Gamma\left(1 + \frac{1}{\hat{b}_1}\right) = \hat{a}_2 \Gamma\left(1 + \frac{1}{\hat{b}_2}\right) \tag{40}$$

a_1 is the initial scale parameter and a_2 is the new scale parameter. The gamma function can be simplified as

$$\Gamma(1 + \delta) \approx \sqrt{2\pi} \mathrm{e}^{-\delta} \delta^{\delta + \frac{1}{2}} \tag{41}$$

by considering $\theta + \frac{1}{2} \approx 1$ (Abramowitz and Stegun 1972). Hence

$$\Gamma\left(1 + \frac{1}{\hat{b}_1}\right) \approx \frac{1}{\hat{b}_1} \sqrt{2\pi} \times \exp\left(-\frac{1}{\hat{b}_1}\right) \tag{42}$$

δ is a reciprocal for the shape factor $\left(\frac{1}{\hat{b}}\right)$ and π is the Archimedes constant. To ensemble the cell runoff transfer, a cell to outlet superposition algorithm is used to generate the unit response of the catchment. Volumetric inflow to each cell (m^3) can be calculated as

$$V_{\mathrm{f}} = 0.001 \times A_{\mathrm{p}} \times P_{\mathrm{e}} \tag{43}$$

A_{p} is the pixel area (m^2) and is P_{e} rainfall depth (mm). A composite hydrograph is constructed in such a way that the total volume of flood ($V_{\mathrm{t_1,t_2}}$) at each time interval equals the sum of the areas under the curve. For known a and b, volume $V_{\mathrm{t1,t2}}$ is given by

$$V_{\mathrm{t_1,t_2}} = \frac{V_{\mathrm{f}}}{\exp\left(\left(\frac{t_1}{a}\right)^b\right)} - \frac{V_{\mathrm{f}}}{\exp\left(\left(\frac{t_2}{a}\right)^b\right)} \tag{44}$$

The contribution of groundwater to baseflow is obtained from following equation (Wang et al. 2011; Willems 2009),

$$q_{\mathrm{bg}(t)} = q_{\mathrm{bg}(t-1)} \exp\left(-\frac{t}{60 \times \mathrm{RC}_3}\right) + R_{g(t)}\left(1 - \exp\left(-\frac{t}{60 \times \mathrm{RC}_3}\right)\right) \tag{45}$$

where $q_{bg(t)}$ is groundwater baseflow (m^3/s), $q_{bg(t-1)}$ is groundwater baseflow at the previous time step (m^3/s), $R_{g(t)}$ is the infiltrated water that contributes to baseflow (m^3/s) and RC_3 is the groundwater recession time (h).

The model was tested for two different types of applications. As a first case, the developed model is applied to the Open-Book catchment. The second application is for a mountainous catchment with more complex hydrological processes.

2.2 Applications

2.2.1 Open-Book catchment

The first application of the RASAM model is carried out using a benchmark problem for runoff modelling called the two-dimensional 'Open-Book (V-Shaped) catchment' (Di Giammarco et al. 1996) (Fig. 5). A hypothetical event with an 1.5-h duration has been simulated for a storm with an intensity of 10.8 mm/h using a 2 min time step. Manning's coefficient is 0.15 for both planes and 0.015 (in SI units) for the stream channel. Resolution of the grid is 10 m by 10 m. The surface of both rectangular sides and the middle channel are impervious.

2.2.2 Upper Tarqui catchment

The dataset for the second case study was collected from the Cumbe and Portete stations (Table 4) in the upper Tarqui Catchment in Ecuador (Fig. 6). The stations are representative for a catchment with an area of 202.3 km^2. The upper Tarqui catchment is part of the Paute River catchment, an Andean mountain catchment situated in the southern part of Ecuador, physically characterized by steep slopes, high variability of altitude, rainfall and temperature (Celleri et al. 2007). As the majority of the Andean catchments in Ecuador, the upper Tarqui Catchment is susceptible to the occurrence of flash floods as a result of the presence of steep slopes and permanently saturated soils located over 3500 m above sea level (asl) (Fig. 7).

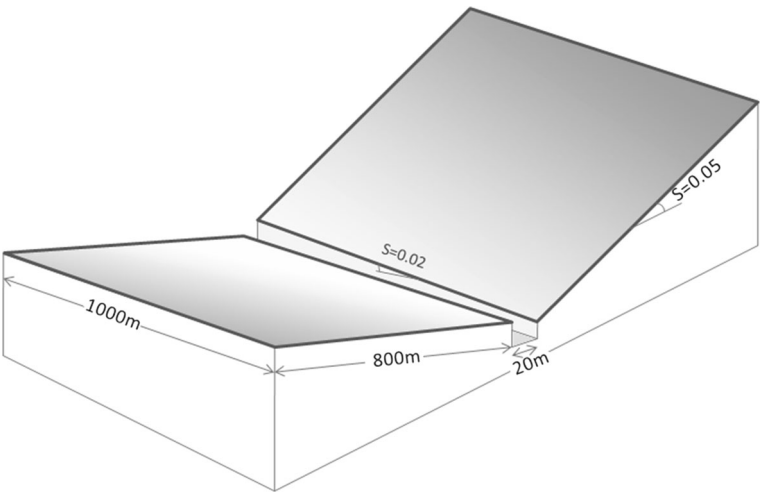

Fig. 5 Geometry and shape of the classical symmetrical Open-Book catchment

3 Results

3.1 Applications

The results for the Open-Book catchment are presented in Fig. 8. The model results are compared with three hydrological models including HydroGeoSphere (Aquanty Inc. 2013), CVFEM (Di Giammarco et al. 1996), IFDM (Di Giammarco et al. 1996) and an analytical solution (Shen and Phanikumar 2010). Results of the implementation in the Open-Book catchment (all last three methods are very similar but an analytical solution is selected as reference) show that consideration of the lag time of the upstream catchment has improved the performance of the model (Table 5; Fig. 8). The volume and peak of the hydrograph are captured by the model, but both scenarios show an early falling limb. The shape of the simulated hydrographs is in agreement with the other hydrological models (Fig. 8).

Figures 9, 10, 11 and 12 show the results of application of the model on four flood events in the upper Tarqui catchment. In response to rainfall most of the events have multiple peaks. The simulations capture the smaller peaks, but the model performs poorly in capturing the highest peaks. A direct correspondence to rainfall can be seen from the simulated graphs.

The event of 6 August 2001 (Fig. 9) is a case with peak underestimation. The response of the observed event was very fast and steep after the measured rainfall. While simultaneous peaks occur during flash flood responses, RASAM shows reaction to the observed rainfall. Event 19 February 2008 (Fig. 10) shows a good similarity during most part of the hydrograph except for the second peak. The behaviour of the event of June 2010 seems similar to the event of 6 August 2001 (Fig. 11). For the event of 25 March 2011 (Fig. 12), the rising limb of the hydrograph has been captured by the model but the falling limb was overestimated.

The resulting hydrographs for both applications were compared with analytical solutions (for Open-Book catchment) and observed streamflows of the upper Tarqui River (Fig. 13). The coefficient of determination (r^2) and the Nash–Sutcliffe Efficiency (EC_{NS}) (Nash and Sutcliffe 1979) for the events of the upper Tarqui River catchment are presented in Table 6. The period of 8/1/2009–4/3/2012 was chosen as validation period with a daily time step ($EC_{NS} = 0.60$).

3.2 Sensitivity analysis

To identify the sensitive parameters and have a better insight in the effect of change in inputs on the outputs, a sensitivity analysis was performed (Table 7). The procedure was done by systematically changing the parameters by $\pm 10\,\%$ (Jain and Singh 2005). The sensitivity analysis shows that the most sensitive parameter of the model is the shape

Table 4 Characteristics of rainfall and discharge stations in the Upper Tarqui Catchment

Station	Longitude (°)	Latitude (°)	Altitude (m)	Type	Gap (%)	Duration years	Daily mean	Std dev
Tarqui DJ Cumbe	−79.05	−3.04	2630	Discharge	0.8	14.3	1.5	2.0
Tarqui DJ Cumbe	−79.05	−3.04	2630	Rainfall	0	14.4	2.3	4.4
Portete	−79.09	−3.14	3174	Rainfall	1.1	14.3	3.1	5.5

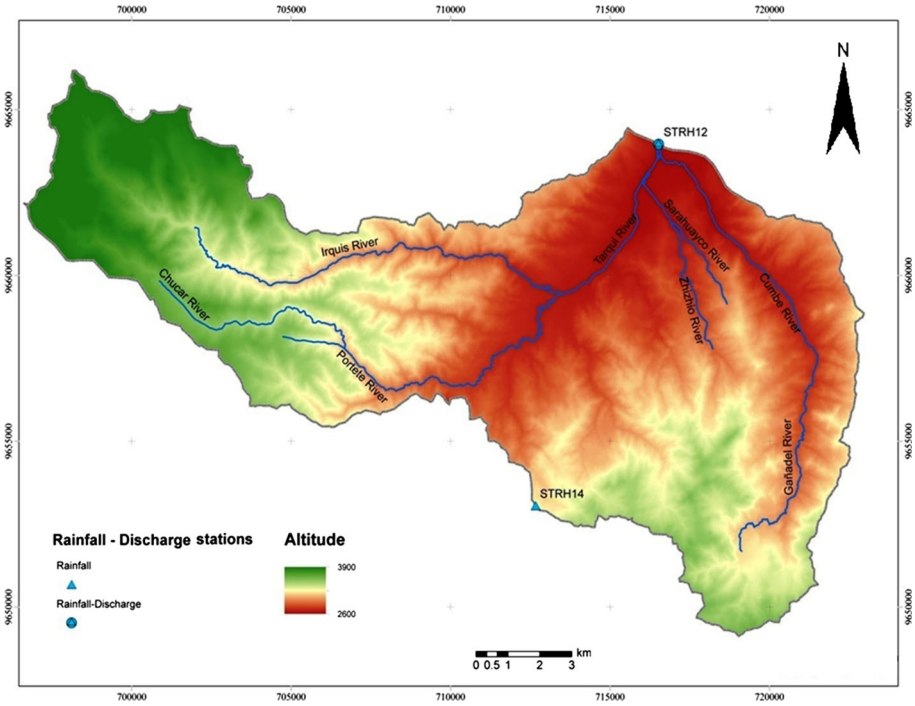

Fig. 6 Topography of the upper Tarqui catchment

parameter. The sensitivity of the shape parameter in the region near to one (such as 1.02) is high so that small changes in the shape parameter results in sharp changes in the form of the hydrograph.

Given that the shape factor itself is a function of time to peak and peak discharge of the pixel (Eq. 35), the parameter is time and space dependent. On the other hand, both time to peak and peak flow are related to lag time hence dependency on intensity is expected. To demonstrate the impact of intensity of rain on the model responses, four different rainfall intensities are presented in Fig. 14. Simulated runoff directly responds to increment of the intensity. Overall, the model is not very sensitive to rainfall intensity.

4 Discussion

Previous studies have demonstrated that the functional similarity between ES and HS could be used as a tool for flood modelling (Collier 1998). This work presents a framework that describes how the operation of hydrological components can be assessed with resistance–capacitance circuits in a spatially distributed way. Here, we discuss the two applications of the model. The first test was performed on the benchmark Open-Book catchment for single and multiple resistance–capacitance circuits. As expected, the multiple resistance–capacitance implementations provide better performance than a single resistance–capacitance implementation. In general, behaviour of the multi-resistance–capacitance model to the input impulse catchment is similar to other hydrological models (Fig. 8). Considering the

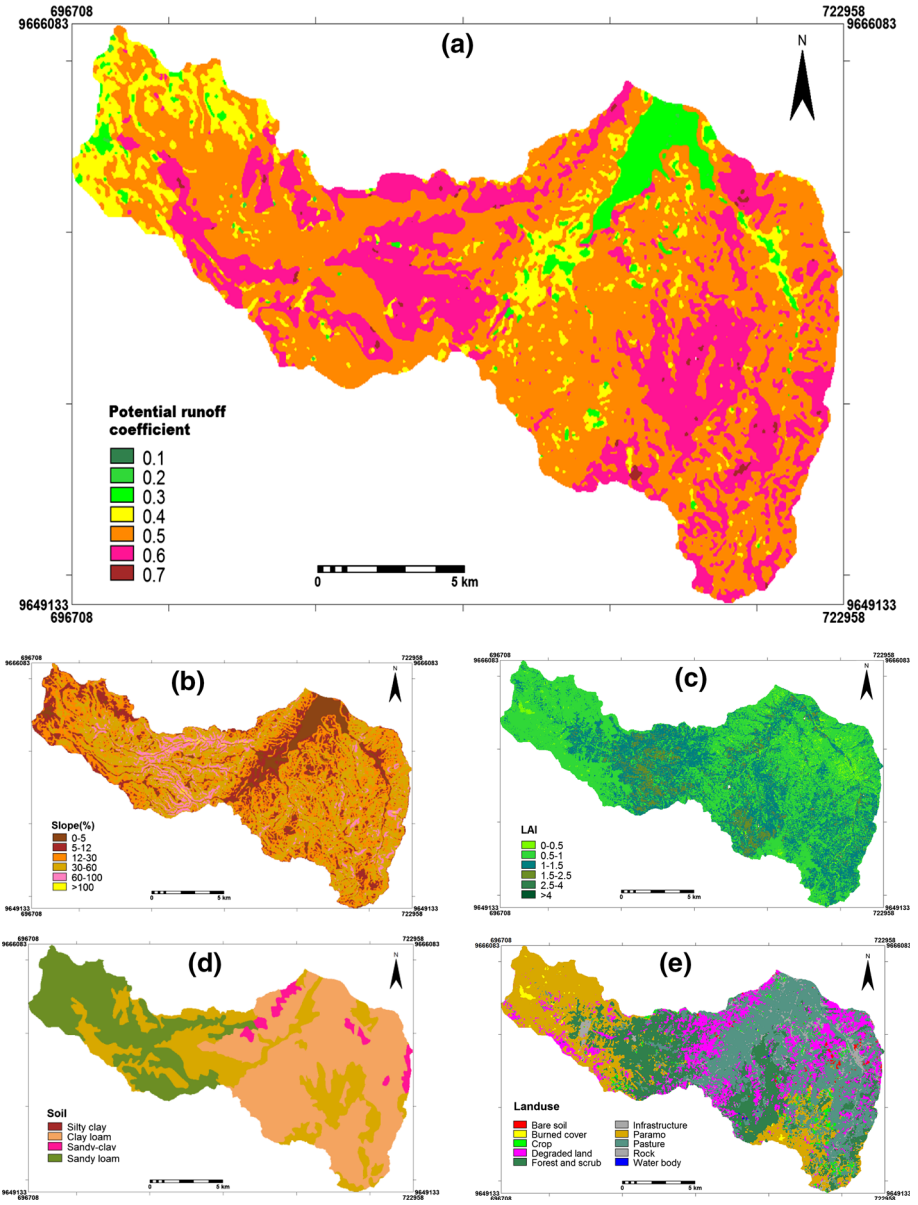

Fig. 7 Potential runoff coefficient and influencing factors for the Upper Tarqui catchment

Open-Book catchment as a single resistance–capacitance, one can state that the time to peak of the hydrograph is around five times as big as the time constant of the corresponding resistance–capacitance (Fig. 1a). The timing characteristics (time to peak and lag time) of the catchment are directly responsible for the rising limb of the hydrograph at the outlet of the Open-Book catchment. The study shows that with a uniform unit of rainfall, before the

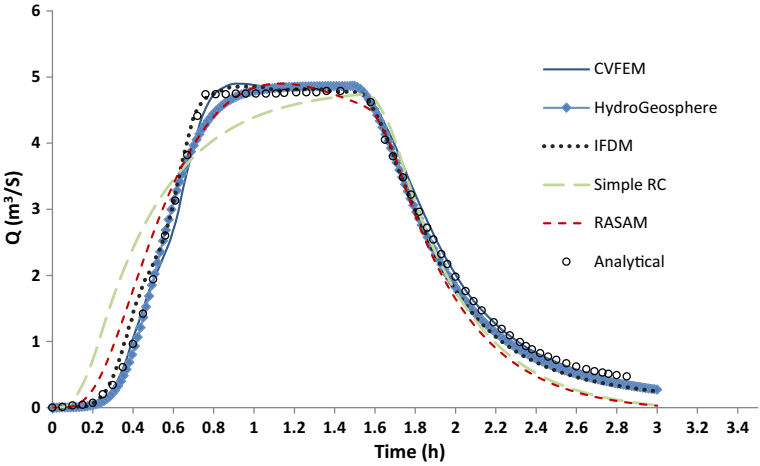

Fig. 8 The RASAM simulation for the Open-Book catchment event of a 1.5-h rainfall, good agreement is shown with other hydrological models: CVFEM (Di Giammarco et al. 1996), HydroGeoSphere (Aquanty Inc. 2013), IFDM (Di Giammarco et al. 1996) and the analytical solution (Shen and Phanikumar 2010)

Table 5 Efficiency criteria (coefficient of determination r^2 and Nash–Sutcliffe EC_{NS}) for Open-Book catchment simulations

Event	r^2	EC_{NS}
Single RC	0.93	0.88
Multi-RC (RASAM)	0.96	0.96

lag time the catchment stores water on its surface. The gradient of the falling limb of the hydrograph depends on the amount of this storage.

Because the Open-Book catchment has an impervious surface, there is no baseflow component involved in this model concept. With this same set-up, the model was able to capture the peak, but for the second application for the upper Tarqui catchment, the peaks were underestimated. Particularly, the occurrence of the multi-peak events was not captured well. Since discharge simulation depends on various factors such as slope, pathway length, Manning's coefficient, losses, intensity and infiltration rates, it is difficult to single out the reason for under performance. But producing a better simulation in the absence of sub-surface processes might be a sign of soil storage processes. It seems there exists a maximum value for storage in the system, which has an important impact on the peak flow, after this threshold flow reaches an equilibrium limit. Earlier studies have reported the impact of antecedent soil moisture on flood generation. Also it can be expected due to the higher complexity of the system that the performance of the simulations for the upper Tarqui catchment is lower than the Open-Book catchment. The steep slopes and high potential runoff coefficients (Fig. 7a) of this catchment lead to a fast basin response. A combination of a shallow soil with high water retention capacity and the presence of steep slopes in the studied catchment may explain the existence of multiple peaks and flash floods in the catchment. The soil moisture conditions seem to be crucial for appropriate estimation of discharge during high flood events. For those events occurring at the

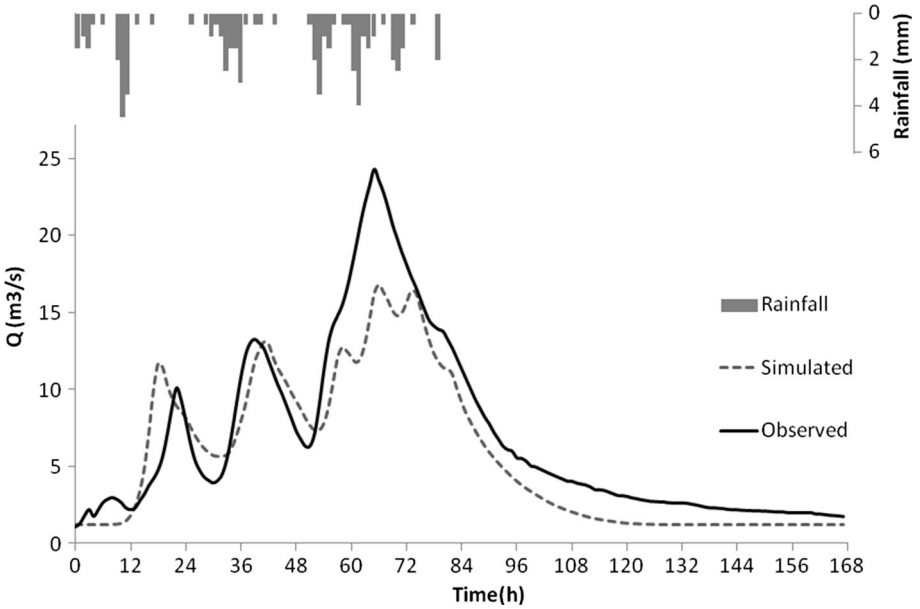

Fig. 9 Observed and simulated hydrographs for the upper Tarqui River, Ecuador for the event of 6 August 2001

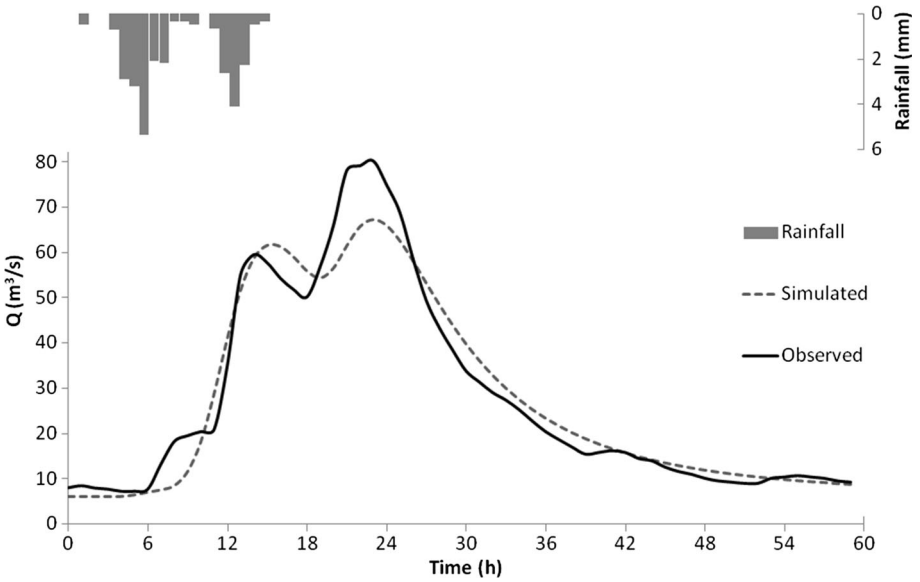

Fig. 10 Observed and simulated hydrographs for the upper Tarqui River, Ecuador for the event of 19 February 2008

beginning of the rainy season, the estimation of peaks seems better than other events for which the soil moisture was higher. Poor performance in the second peak of the hydrograph can be linked with the soil water storage. Since the model uses the shape parameter

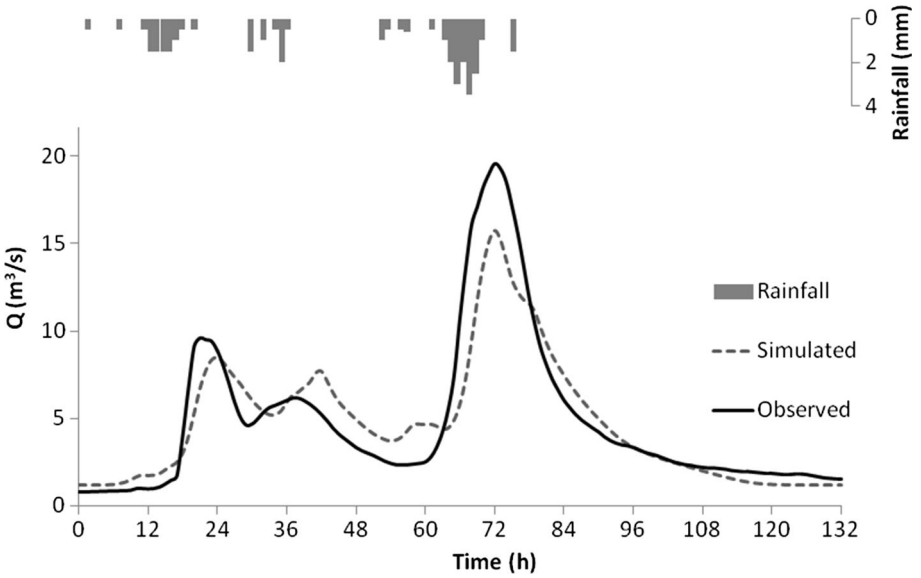

Fig. 11 Observed and simulated hydrographs for the upper Tarqui River, Ecuador for the event of 18 June 2010

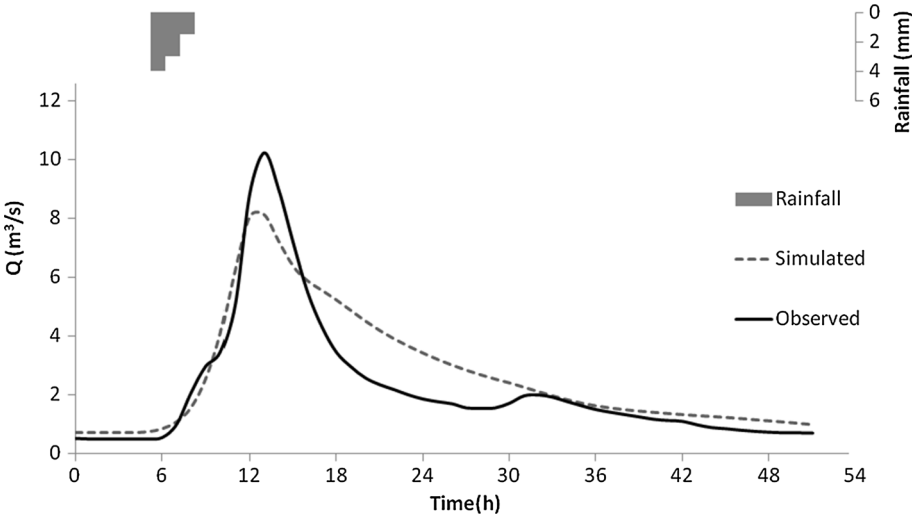

Fig. 12 Observed and simulated hydrographs of Upper Tarqui River, Ecuador for the event of 25 March 2011

for calibration, another possible reason for low performance in simulation of the multiple peaks can be related to the fact that if a hydrograph has a second or third peak it is difficult to fit a shape parameter on the observed data. Referring to the analogy, the pattern of charging and discharging might be responsible for the sharpness of the catchment response (e.g. May 1998 in Fig. 13). Under the condition that soil storage is fully charged,

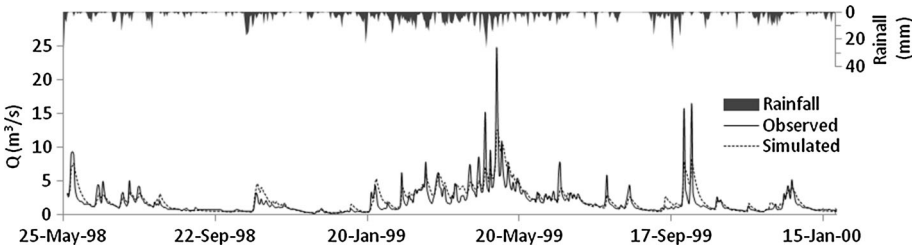

Fig. 13 Rainfall, observed and simulated discharge for Upper Tarqui River, Ecuador for the period 28/05/1998–04/08/1999

Table 6 Efficiency criteria (coefficient of determination r^2 and Nash–Sutcliffe EC_{NS}) for hourly and daily simulations

Event	Time step	Start time	r^2	EC_{NS}
Event 1	Hourly	6/8/2001 23:00	0.86	0.55
Event 2	Hourly	19/02/2008 8:00	0.95	0.95
Event 3	Hourly	6/18/2010 12:05	0.86	0.88
Event 4	Hourly	3/25/2011 9:00	0.85	0.78
Continuous series	Daily	28/05/1998–04/08/1999	0.76	0.68

Table 7 Sensitivity of the RASAM model to various inputs

Parameter name	Symbol	Influencing process	Degree of sensitivity
Shape parameter	$\hat{b}$	All processes	High
Scale parameter	$\hat{a}$	All processes	Moderate
Rainfall	P	All processes	High
ET	ET	AET, surface runoff	High
Intensity	i	Surface runoff	Low
Interception factor	C_P	Interception, surface runoff	Moderate
Leaf area index	LAI	Interception	Moderate
Surface storage factor	S	Surface runoff, infiltration	Moderate
Dimensionless drainage factor	k_{in}	Interflow	High
Runoff length	L	Surface runoff, interflow	Moderate
Recession factor	k_g	Groundwater	High
n Manning	n	Surface runoff	Moderate
Slope	S_l	Surface runoff, interflow	Low
Curve number	CN	Surface runoff, infiltration	Moderate

infiltration reaches its minimal rate. It is also likely that the charged storage contributes to outflow.

Recently Guzman et al. (2015) showed that subsurface hydrological processes in the Tarqui basin are related to releasing stored water in the soils, especially in the Paramos, a predominant ecosystem at high elevations with grassland coverage. Despite the diversity of

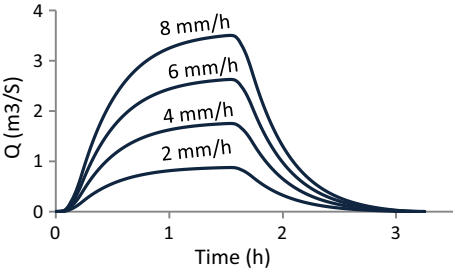

Fig. 14 Simulated response of the Open-Book catchment to different rainfall intensities

geological formations and significant changes in the topography, the soils in Paramos are quite homogeneous (Buytaert et al. 2006). This landscape is characterized by high water retention and saturated hydraulic conductivity (Guzman et al. 2015). The existence of such extensive storage capacity is important for interflow processes in the catchment. RASAM uses a simplified interflow that depends on the saturated hydraulic conductivity. In addition to the above-mentioned reasons for mismatch between the simulated results and observed discharges, uncertainties in the model structure and input data should be taken into account. Another reason for the underestimation of discharge might be related to the spatial variability of rainfall and its representation in the model. Due to the limited number of available rain gauge stations in the upper Tarqui catchment, the Thiessen polygons method was used for weighting the distribution of rainfall in the catchment. The two used rainfall stations are likely to not fully be representative for the spatial variability of rainfall; the average rainfall might have led to underestimation of discharge, especially when highly intensive rainfall events are not evenly distributed within the catchment.

The Weibull distribution has proven to be a useful tool for modelling the flood hydrograph. This is in line with Pramanik et al. (2010) who used probability density functions of the Weibull distribution to estimate discharge. One advantage of this formulation is the availability of the area under the Weibull curve (Eq. 43), which allows calculation of the discharge at a specific time. The shape and scale parameters make it flexible for parameterization.

5 Conclusion

A new spatially distributed model based on electric circuit analogy is introduced for flood modelling. The governing equations for water balance components at pixel scale are described using exponential functions expressing the similarity with ES and the nonlinearity of the system. Because of the strong similarity, the electrical principles are applicable in hydrological equivalents, but modification is required to translate the problem and simplify the complexity of modelling. To simulate the dynamic nature of floods, cells of a raster grid are modelled through the analogy of equivalent RC circuits. By borrowing the theory from electrical science, RASAM simplifies the cell response to a pair of shape and scale parameters of the Weibull distribution. The watershed scale analysis of Rai et al. (2009) on different watersheds having different size, climate and physiographic characteristics showed that shape parameter varies from 0.99 to 2.54. The higher shape factor produces sharper hydrograph. The scale parameter is responsible for time to peak. It can be noticed that under a certain conditions, the formulated approach corresponds to the NRCS

dimensionless unit hydrograph, while the rising curve was slightly earlier and falling limb occurrence was faster. An advantage the dimensionless technique is the shape of the output hydrograph can be calibrated easily.

For the second application, the model is tested in the upper Tarqui watershed (Ecuador) against observed hydrographs. Using a dimensionless Weibull hydrograph, a synthetic hydrograph of each cell was constructed which resulted in the response function of the catchment. The derived hydrograph shows that the model is able to reproduce flood hydrographs. The simulated hydrographs show an early start compared to the observations, but by taking the effect of lag time into account simulations have been improved.

The model approach exploits the dualism between a hydrological system and the analogue electrical network. From the two applications, we can conclude that the analogy sheds light on the simplification of the water balance at pixel level by representing hydrological processes as RC circuits. An advantage of the presented methodology is that it allows splitting and representing catchment scale hydrological processes into smaller meaningful components. On the other hand, it has the capability to simulate the functionality of basin-scale systems by interrelating between hydrological components. For future work, it is recommended to perform an extensive model comparison and evaluation study to compare RASAM model results with results from other hydrological models for hydrologically different real basins.

References

Abramowitz M, Stegun IA (1972) Handbook of mathematical Functions with Formulas, Graphs, and Mathematical Tables. Dover Publications, New York

Agarwal K, Sylvester D and Blaauw D (2003) Simple Metrics for Slew Rate of RC Circuits Based on Two Circuit Moments. Proceedings of the 40th annual Design Automation Conference (DAC): 950-953

Amengual A, Romero R, Gomez M, Martin A, Alonso S (2007) A hydrometeorological modelling study of a flash-flood event over Catalonia, Spain. J Hydrometeorol 8:282–303

Anquetin S, Yates E, Ducrocq V, Samouillan S, Chancibault K, Davolio S, Buzzi A (2005) The 8 and 9 September 2002 flash flood event in France: a model intercomparison. Nat Hazards Earth Syst Sci 5:741–754

Anquetin S, Braud I, Vannier O, Viallet P, Boudevillain B, Creutin JD, Manus C (2010) Sensitivity of the hydrological response to the variability of rainfall fields and soils for the Gard 2002 flash-flood event. J Hydrol 394(1):134–147

Aston AR (1979) Rainfall interception by eight small trees. J Hydrol 42:383–396

Barredo JI (2007) Major flood disasters in Europe: 1950–2005. Nat Hazards 42(1):125–148

Berz G, Kron W, Loster T, Rauch E, Schimetschek J, Schmieder Siebert A, Smolka A, Wirtz A (2001) World map of natural hazards—a global view of the distribution and intensity of significant exposures. Nat Hazards 23(2–3):443–465

Bhunya PK, Berndtsson R, Ojha CSP, Mishra SK (2007) Suitability of gamma, chisquare, synthetic unit hydrographs. J Hydrol 334:28–38

Blöschl G, Reszler C, Komma J (2008) A spatially distributed flash flood forecasting model. Environ Model Softw 23(4):464–478

Brath A, Rosso R (1993) Adaptive calibration of a conceptual model for flash flood forecasting. J Water Resour Res 29(8):2561–2572

Borga M, Boscolo P, Zanon F, Sangati M (2007) Hydrometeorological analysis of the 29 August 2003 flash flood in the Eastern Italian Alps. J Hydrometeorol 8(5):1049–1067

Buytaert W, Celleri R, De Bievre B, Cisneros F, Wyseure G, Deckers J, Hofstede R (2006) Human impact on the hydrology of the Andean Paramos. Earth Sci Rev 79(1):53–72

Cannon RHJ (1967) Dynamics of physical systems. McGraw-Hill, New York

Celleri R, Willems P, Buytaert W, Feyen J (2007) Space–time rainfall variability in the Paute Basin, Ecuadorian Andes. Hydrol Process 21(24):3316–3327

Chow VT (1964) Hydrology and its development. In: Handbook of applied hydrology, McGraw-Hill, New York, Section 1:1–10
Collier CG (1998) Modelling a river catchment using an electrical circuit analogue. Hydrol Earth Syst Sci 2:9–18
Costa JE (1987) Hydraulics and basin morphometry of the largest flash floods in the conterminous United States. J Hydrol 93:313–338
De Jong SM, Jetten VG (2007) Estimating spatial patterns of rainfall interception from remotely sensed vegetation indices and spectral mixture analysis. Int J Geogr Inf Sci 21(5):529–545
Di Giammarco P, Todini E, Lamberti P (1996) A conservative finite elements approach to overland flow: the control volume finite element formulation. J Hydrol 175(1):267–291
Ferraris L, Rudari R, Siccardi F (2002) The uncertainty in the prediction of flash floods in the Northern Mediterranean environment. J Hydrometeorol 3:714–727
Foody GM, Ghoneim EM, Arnell NW (2004) Predicting locations sensitive to flash flooding in an arid environment. J Hydrol 292(1):48–58
Gabellani S, Silvestro F, Rudari R, Boni G (2008) General calibration methodology for a combined Horton-SCS infiltration scheme in flash flood modelling. Nat Hazards Earth Syst Sci 8(6):1317–1327
Garrote L, Bras RL (1995) A distributed model for real-time flood forecasting using digital elevation models. J Hydrol 167(1–4):279–306
Gaume E, Livet M, Desbordes M, Villeneuve JP (2004) Hydrologic analysis of the Aude, France, flash flood 12 and 13 November 1999. J Hydrol 286:135–154
Georgakakos KP (1986) On the design of natural, real-time warning systems with capability for site-specific, flash flood forecasts. Bull Am Meteorol Soc 67:1233–1239
Guzman P, Batelaan O, Huysmans M, Wyseure G (2015) Comparative analysis of baseflow characteristics of two Andean catchments, Ecuador. Hydrol Process 29(14):3051–3064
Hapuarachchi HAP, Wang QJ, Pagano TC (2011) A review of advances in flash flood forecasting. Hydrol Process 25(18):2771–2784
Horton RE (1933) The role of infiltration in the hydrologic cycle. Trans Am Geophys Union 14:446–460
Hoyningen-Huene JV (1981) Die Interzeption des Niederschlags in landwirtschaftlichen Pflanzenbeständen. Arbeitsbericht Deutscher Verband fur Wasserwirtschaft und Kulturbau. DVWK, Braunschweig
Inc Aquanty (2013) HGS 2013, HydroGeoSphere user manual. Waterloo, Ontario
Jain MK, Singh VP (2005) DEM-based modelling of surface runoff using diffusion wave equation. J Hydrol 302(1):107–126
Jarrett RD (1987) Errors in slope-area computations of peak discharges in mountain streams. J Hydrol 96(1):53–67
Jonkman SN (2005) Global perspectives on loss of human life caused by floods. Nat Hazards 34(2):151–175
Kundzewicz ZW (1987) Electro-hydrological analogies. In: Water for the future: hydrology in perspective, vol 164. IAHS Publication, 55–66
Laraque A, Ronchail J, Cochonneau G, Pombosa R, Guyot JL (2007) Heterogeneous distribution of rainfall and discharge regimes in the Ecuadorian Amazon basin. J Hydrometeorol 8(6):1364–1381
Liu F, Kashyap C, Alpert CJ (2002) A delay metric for RC circuits based on the Weibull distribution, Proceedings of the IEEE/ACM International Conference on Computer Aided Design, pp 620-624
Marchi L, Borga M, Preciso E, Gaume E (2010) Characterisation of selected extreme flash floods in Europe and implications for flood risk management. J Hydrol 394:118–133
Mariani S, Casaioli M, Accadia C, Llasat MDC, Pasi F, Davolio S, Buzzi A (2005) A limited area model intercomparison on the" Montserrat-2000" flash-flood event using statistical and deterministic methods. Nat Hazards 5(4):565–581
Melesse AM, Weng Q, Thenkabail PS, Senay GB (2007) Remote sensing sensors and applications in environmental resources mapping and modelling. Sensors 7(12):3209–3241
Nash JE, Sutcliffe JV (1979) River flow forecasting through conceptual models 1: a discussion of principles. J Hydrol 10:282–290
Norbiato D, Borga M, Sangati M, Zanon F (2007) Regional frequency analysis of extreme precipitation in the eastern Italian Alps and the August 29, 2003 flash flood. J Hydrol 345:149–166
Nourani V, Monadjemi P (2006) Laboratory simulation of a geomorphological runoff routing model using liquid analog circuits. J Environ Hydrol 14:1–9
Nourani V, Monadjemi P, Singh VP (2007) Liquid analog model for laboratory simulation of rainfall-runoff process. J Hydrol Eng 12(3):246–255
Nourani V, Aminfar MH, Alami MT, Sharghi E, Singh VP (2014a) a) Unsteady 2-D seepage simulation using physical analog, case of Sattarkhan embankment dam. J Hydrol 519:177–189
Nourani V, Aminfar MH, Alem MT, Shargi E (2014b) b) Liquid analog circuits for laboratory simulation of steady-state seepage. J Environ Hydrol 22(2):1–15

Oudin L, Moulin L, Bendjoudi H, Ribstein P (2010) Estimating potential evapotranspiration without continuous daily data: possible errors and impact on water balance simulations. Hydrol Sci J (Journal des Sciences Hydrologiques) 55(2):209–222

Pedersen JT, Peters JC, Helweg OJ (1980) Hydrographs by single linear reservoir model. No. HEC-TP-74. J Hydraulics Div-CA, ASCE 106(HY5):837–852

Pramanik N, Panda RK, Sen D (2010) Development of design flood hydrographs using probability density functions. Hydrol Process 24(4):415–428

Rai RK, Sarkar S, Singh VP (2009) Evaluation of the adequacy of statistical distribution functions for deriving unit hydrograph. Water Resour Manag 23(5):899–929

Rawlins MA, Nicolsky DJ, McDonald KC, Romanovsky VE (2013) Simulating soil freeze/thaw dynamics with an improved pan-Arctic water balance model. J Adv Model Earth Syst 5(4):659–675

Reed S, Schaake J, Zhang Z (2007) A distributed hydrologic model and threshold frequency-based method for flash flood forecasting at ungauged locations. J Hydrol 337(3):402–420

Ruiz-Villanueva V, Díez-Herrero A, Stoffel M, Bollschweiler M, Bodoque JM, Ballesteros JA (2010) Dendrogeomorphic analysis of flash floods in a small ungauged mountain catchment (Central Spain). Geomorphology 118(3):383–392

Schreiber P (1904) Uber die Beziehungen zwischen dem Niederschlag und der Wasserführung der Flube in Mitteleuropa. Z fur Meteorologie 21:441–452

Sheikh V, Visser S, Stroosnijder L (2009) A simple model to predict soil moisture: bridging Event and Continuous Hydrological (BEACH) modelling. Environ Model Softw 24(4):542–556

Shen J (1965) Use of analogue models in the analysis of flood runoff. U.S. Geological Survey Professional Paper 506-A:1- 24

Shen C, Phanikumar MS (2010) A process-based, distributed hydrologic model based on a large-scale method for surface–subsurface coupling. Adv Water Resour 33(12):1524–1541

Sherman LK (1932) Streamflow from Rainfall by the Unit Graph Method. Eng News Record 108:501–505

Stark CP, Stark GJ (2001) A channelization model of landscape evolution. Am J Sci 301(4–5):486–512

USDA-SCS (1985) National Engineering Handbook. Section 4: Hydrology, Washington DC

Valiantzas JD (2006) Simplified versions for the Penman evaporation equation using routine weather data. J Hydrol 331:690–702

Wang QJ, Pagano TC, Zhou SL, Hapuarachchi HAP, Zhang L, Robertson DE (2011) Monthly versus daily water balance models in simulating monthly runoff. J Hydrol 404(3):166–175

Weibull W (1951) A statistical distribution function of wide applicability. J Appl Mech 18:293–297

Willems P (2009) A time series tool to support the multi-criteria performance evaluation of rainfall-runoff models. Environ Model Softw 24(3):311–321

Yates D, Warner TT, Brandes EA, Leavesley GH, Sun JZ, Mueller CK (2001) Evaluation of flash-flood discharge forecasts in complex terrain using precipitation. J Hydrol Eng 6(4):265–274